Primary objective grating telescopy: optical properties and feasibility of applications

Leaf Swordy,[a] Heidi Jo Newberg,[a,*] and Thomas Ditto[a,b]
[a]Rensselaer Polytechnic Institute, Department of Physics, Applied Physics, and Astronomy, Troy, New York, United States
[b]3DeWitt LLC, Ancramdale, New York, United States

Abstract. We develop the theoretical foundation for primary objective grating (POG) telescopy. In recent years, a wide range of telescope designs that collect the light over a large grating and focus it with a secondary receiving optic that is placed at grazing exodus have been proposed by Thomas D. Ditto and are sometimes referred to as Dittoscopes. Applications include discovery and characterization of exoplanets, discovery of near-Earth asteroids, and spectroscopic surveys of the sky. These telescopes would have small aerial mass, and therefore, provide a path forward to launch large telescopes into space. Because this series of telescope designs departs from traditional telescope designs, it has been difficult to evaluate which applications are most advantageous for this design. We define a figure of merit, the "spectral étendue," that characterizes the photon collection capability of a POG. It is demonstrated that the diffraction limit for observations is determined by the length of the grating. We evaluate the effects of atmospheric seeing for ground-based applications and the disambiguation of position versus wavelength in the focal plane using a second dispersing element. Finally, some strategies for fully reaping the benefits of POG optical characteristics are discussed. [DOI: 10.1117/1.JATIS.9.2.024001]

Keywords: primary objective gratings; astronomy; space optics; diffractive optics; telescopes; gratings.

Paper 22073G received Jul. 15, 2022; accepted for publication Mar. 10, 2023; published online Apr. 4, 2023.

1 Introduction

The concept of large-scale space telescopes consisting of thin-film optical holograms has garnered interest since the advent of optical holography in the 1960s.[1] The typical application is that of a large diameter Fresnel zone plate (FZP) or photon sieve, with proposed applications seeking to solve problems associated with UV optics and large space apertures with low aerial mass. Development of these technologies stagnated after the 1960s, likely due to promising advances in UV/IR optics coupled with the highly chromatic behavior of holographic primaries. More recently, interest in large-aperture thin-film holographic primaries has undergone a resurgence, following the development of the dispersion-corrected Fresnel lens.[2,3]

Throughout the late 1990s and early 2000s, many different thin-film space observatories were proposed[4–7] and explored to various degrees of development. Such designs feature extremely large apertures with low aerial mass and less susceptibility to typical figure errors than conventional telescopes. The primary drawback with many of the proposed concepts is found in the extremely long focal lengths they incorporate. Long focal lengths are needed in order to correct for chromatism and achieve low-surface figure requirements, this topic is discussed in Hyde EYEGLASS.[4] These focal lengths are often on the scale of kilometers, requiring precise formation flying of many optical components.

The topic of this publication differs from the preceding discussion in that, rather than an FZP or photon sieve, the primary optical element is imagined as a large area diffraction grating at grazing exodus, subsequently viewed by a secondary telescope or camera. Placing a grating in

*Address all correspondence to Heidi Jo Newberg, newbeh@rpi.edu

front of the aperture of a telescope is not a new concept in and of itself; prior to the advent of optical fiber spectroscopy, such techniques, generally referred to as slitless spectroscopy, were commonplace.[8] The focal plane images obtained with slitless spectroscopy are similar to the more modern technique of using a grism to obtain so called "grism images." In a grism image, each object in the focal plane is spread out into a small spectrum, thereby allowing for rudimentary spectral analysis of many objects simultaneously. The use of a diffraction grating as a primary objective dates to the very beginning of 20th century astronomy.[9] The spectra obtained with such techniques are generally low resolution, with higher resolution limited by spreading and obfuscation of objects in the focal plane. Thus the advent of astronomical fiber spectroscopy in the late 1970s[10] has resulted in fewer applications utilizing primary objective grating (POG) spectroscopy. The optical designs discussed here differ from a traditional grism image due to the high exodus angle in which light is collected from the grating. This subtle change results in a wide array of interesting (and sometimes counterintuitive) optical properties.

Inspiration for this publication is drawn from more recent realizations by Thomas D. Ditto. Beginning in the early 2000s,[11] Ditto formulated unique telescope architectures featuring dispersive primaries. These eponymous "Dittoscope" architectures are unique from all previous applications, in that they utilize the POG for optical leverage by collecting light from the grating in a grazing exodus configuration and use a secondary spectrograph to disambiguate the overlapping spectra from an enlarged field of view (FOV). Viewing the POG at grazing exodus can result in a massive increase in collection area and angular resolution, and a hugely dispersed spectrum of each object. It will be seen in the details of this publication that a wealth of interesting optical properties arise from the most basic realization of a Dittoscope.

Ditto has proposed many specific designs and applications of POG technology.[12] Current design concepts feature a variety of light collection schemes after diffraction from the grating, with most featuring secondary spectrographic capability to disambiguate dispersed light of focal plane objects. This technique is called "dual dispersion." While consideration of specific applications will be briefly discussed, they are generally outside the scope of this paper.

Presented here is a purely theoretical study of the Dittoscope concept. Although many real-life implementation issues exist, they will only be discussed to a very limited extent in Sec. 6.5. We intend to explore only the most basic optical properties of a POG in grazing exodus configuration, often modeling the secondary focusing element as a mere aperture-mirror combination of little description. The results and derivations herein are only applicable for gratings operating in the first diffraction order; complications arising from higher and negative orders are not discussed in detail. It is the goal of this publication to place the general properties of such an arrangement on a firm foundation. The optical geometry of arbitrary systems and configurations are discussed with the goal of establishing relationships among the light collection area, FOV, bandwidth, and angular resolution. New relationships and figures of merit are described, facilitating comparison between theoretical POG architectures and contemporary observational techniques.

We show that grazing exodus POG configurations present many potential benefits, including extremely large light collection area, high spectral/angular resolution, a massively enhanced FOV, and the potential for low-cost lightweight deployment in space. These serve as the primary motivating factors for this work. The feasibility and potential benefits of grazing exodus POG observatories are discussed.

2 THE MOST

As an introduction to the basic concepts underlying a Dittoscope, we can imagine a polychromatic collimated beam incident on a transmission grating [Fig. 1(a)]. In this scenario, the polychromatic incident beam is output as a spectrum of monochromatic exodus beams, with exodus angles determined by the grating equation:

$$\sin(\theta_{\text{in}}) + \sin(\theta_{\text{out}}) = m\frac{\lambda}{p}, \tag{1}$$

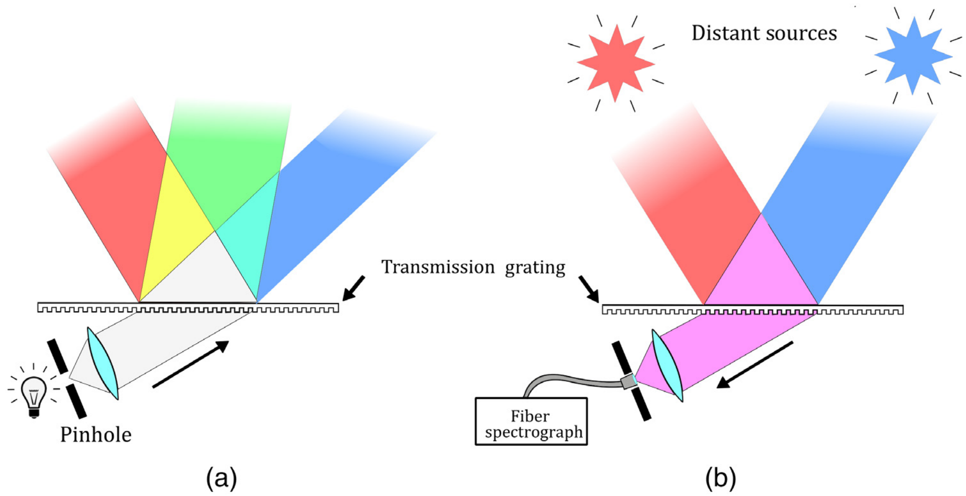

Fig. 1 (a) A broadband source placed behind a pinhole in the focal plane is output as a variety of collimated monochromatic beams. (b) The situation of (a) is reversed, such that collimated input beams from distant sources (e.g., stars in the sky) are received by an optical fiber placed in the focal plane of a receiving lens. Each location in the sky can be received only in a narrow bandwidth, allowing on-sky position to be identified by received wavelength via a spectrograph.

where θ_{in} can be either the angle of incidence of the polychromatic beam [Fig. 1(a)], or the incident angle from a single object in the sky [Fig. 1(b)], θ_{out} is the angle in which light with wavelength λ is diffracted from the grating, m is the diffraction order, and p is the grating pitch.

The two situations shown in Fig. 1 are essentially opposites of one another. In Fig. 1(a), light radiated from a pinhole in the focal plane is output to the field as a spectrum of collimated beams. Conversely, Fig. 1(b) places a single optical fiber in the focal plane, this optical fiber receives field photons at a different wavelength according to the incident angle of the light (location on the sky). The optical arrangement of Fig. 1(b) embodies the most basic aspects of the Dittoscope concept. The arrangement will later be complicated by moving the receiving optics to an extreme angle, and allowing the entire focal plane to receive incident photons (i.e., many fibers/slits).

Now we will discuss a specific Dittoscope design, The High Étendue Multiple Object Spectrographic Telescope (THE MOST).[13,14] THE MOST design (Fig. 2) imagines collecting light from the sky through a large (tens of meters or larger), precision ruled primary objective plane grating. The light from this grating is then focused with a paraboloid mirror or possibly a conventional telescope with a wider corrected FOV (in either case termed a "secondary focusing element"). In the focal plane of the secondary focusing element, the positions of objects in the sky are correlated with the wavelength of the light that is received in the direction of dispersion according to the grating equation [Eq. (1)]. In the direction perpendicular to the dispersion (i.e., oblique incident angles), the angular position of the object observed is unambiguous.

A functional difference between the classical objective prism design and THE MOST is the replacement of the prism with a grating at grazing exodus. This change allows us to image a very large collecting area from a large grating, paired with a much smaller focusing optic. The disambiguation of received photons by a secondary dispersing element (dual dispersion) is also a unique feature. In most cases, the secondary focusing element collects light at an exodus angle approaching $\theta_{out} \rightarrow 90$ deg. This secondary focusing optic could have the optical design of an ordinary optical telescope, which focuses light over a larger FOV than a simple paraboloid mirror. By collecting the light from a large exodus angle, we can "observe" a long grating with a telescope mirror of modest size (due to anamorphic magnification). THE MOST uses the second dispersing element, or spectrograph, to untangle the position in the sky from which each photon originated from the wavelength of the photon that was received. If the position and wavelength were known for all photons received at the focal plane of the secondary, true angular positions of objects in the sky can be found by simple application of the grating equation [Eq. (1)].

The placement of the secondary focusing element at a large angle of diffraction leads to a very high dispersion of the light from the grating. This means that only a small wavelength range

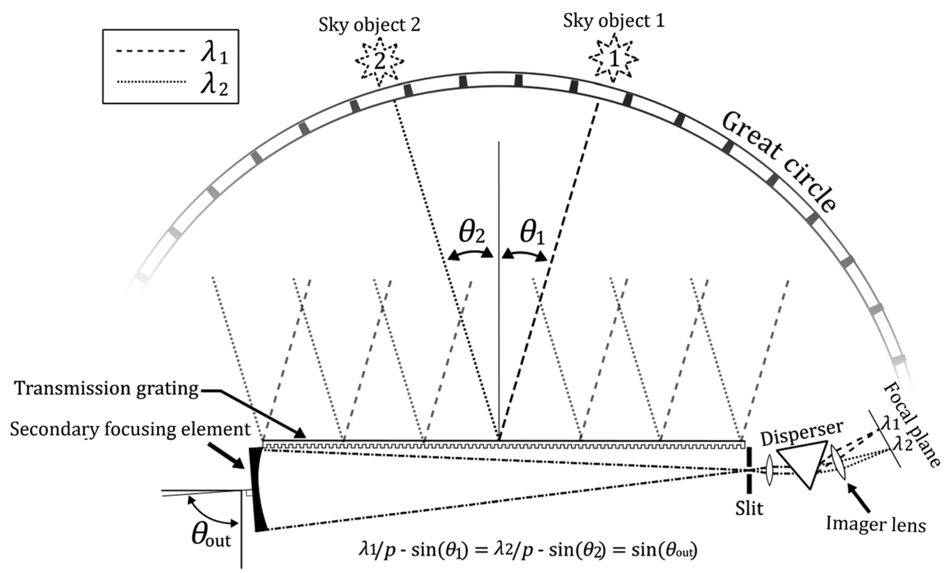

Fig. 2 Configuration of the THE MOST. Incident angles $\theta_{1,2}$ are diffracted into a fixed exodus angle θ_{out} and collected by the paraboloid mirror labeled "secondary focusing element." The secondary focusing element coveys light to a slit located in the focal plane, after which the on-sky position of the incident light is disambiguated by a secondary dispersing element (conceptually represented as a prism). In this arrangement, each unique location in the sky is associated with a unique position in the focal plane and is received in a narrow bandwidth (determined by the resolvance of the primary grating and secondary disperser).

of light from a particular object in the sky is spread across the entire FOV of the secondary focusing element. For an object with an angle of incidence of zero and an angle of diffraction near 90 deg in the first diffraction order, the resolvance is $R = N \approx L/\lambda$ (since $\lambda \rightarrow p$ as the exodus angle approaches 90 deg), where N is the total number of grooves, L is the length of the grating, and λ is the wavelength of the light. For a grating that is 100 m long and a detection wavelength of 500 nm, $R \approx 200{,}000{,}000$. Clearly, the accuracy with which wavelengths can be determined will be limited by real-life limitations, such as optical defects of the grating (groove spacing and regularity), the allowable number of pixels in the focal plane, and the resolvance of the secondary disperser. However, this example provides an idea of how much a Dittoscope spreads out the light from each object.

3 POG Telescope Geometry

Here we explore the optical geometry of POG telescope designs in all generality, with the ultimate goal of determining a useful figure of merit by which to judge POG designs against conventional telescopes.

3.1 *Light Collection Area*

One of the initial selling points for the Dittoscope is the large collecting area of the low aerial mass grating, which requires a much smaller focusing element due to anamorphic magnification. Figure 3(b) demonstrates that a monochromatic plane wave collected by the entire grating at width W is reflected into a grazing exodus angle, resulting in a smaller cross-sectional area of width A at the output. For broadband sources, each wavelength is collected at a different angle within the FOV of the secondary collector. We will postpone such discussions for the time being, instead concentrating on the single-wavelength view of a grating as a telescope analog.

In a sense, a telescope can be thought of as a device that conveys a large input beam at the primary to a narrow output beam at the ocular. An ocular-equipped telescope also has the important property of enhancing angular differences between input sources (conservation of étendue),

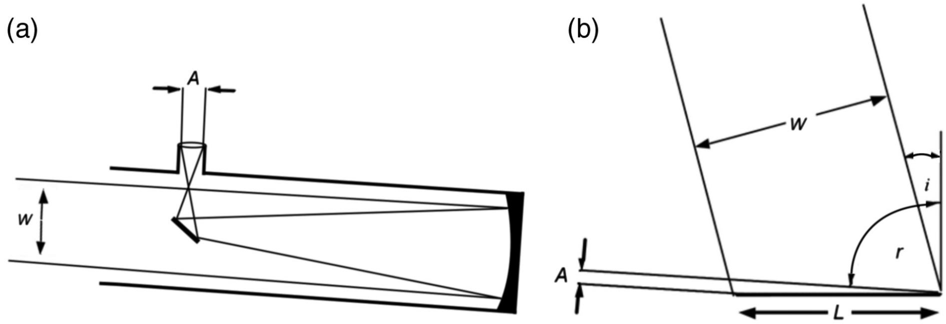

Fig. 3 (a) Conventional Newtonian telescope, conveying input light at width W to the ocular at width A. (b) Anamorphic magnification from a reflection grating, monochromatic light entering at width W is output at width A after diffraction from the grating. The very large cross sectional area at W compared to the received beam A, acts in a similar manner to a conventional telescope in its ability to concentrate light.

so that the diffraction limit incurred by the human pupil may be overcome when making astronomical observations. In Sec. 4, it will be shown that the Dittoscope, in the single-wavelength view, possesses this property as well.

To quantify the enhanced single-wavelength light collection area incurred from a Dittoscope application, we must consider the properties of the secondary focusing element collecting the output light at some central exodus angle. Figure 4 imagines a wide FOV telescope or Schmidt camera observing a grating at high exodus angle, demonstrating that the total area visible to the secondary focusing element is the conic section subtended by its FOV.

The analyses given here utilize circularly symmetric secondary optics. This choice is rather arbitrary and is meant to model the secondary focusing element after the most conventional arrangements of telescopes/cameras. The grating is chosen to be rectangular in all figures as an aid to comprehension. In a practical application, the optics of the secondary might be rectangular in order to utilize the full area of the grating. Conversely, the grating area could be cut down to the elliptical grating area or recorded/etched on an elliptical substrate.

The conic section area depicted in Fig. 4 is the total area visible to the secondary focusing element. Though it will be seen later that each wavelength is collected from a smaller subarea of the overall visible grating area, it is important to quantify this region in order to determine the necessary linear grating dimensions. One of the foci of the ellipse of visible grating area is identified by the intersection of the secondary focusing element optical axis with the grating surface. With one of the foci determined, geometrical properties of the visible grating area, such as the linear eccentricity c, semimajor axis a, and semilatus rectum l, can be derived from trigonometric

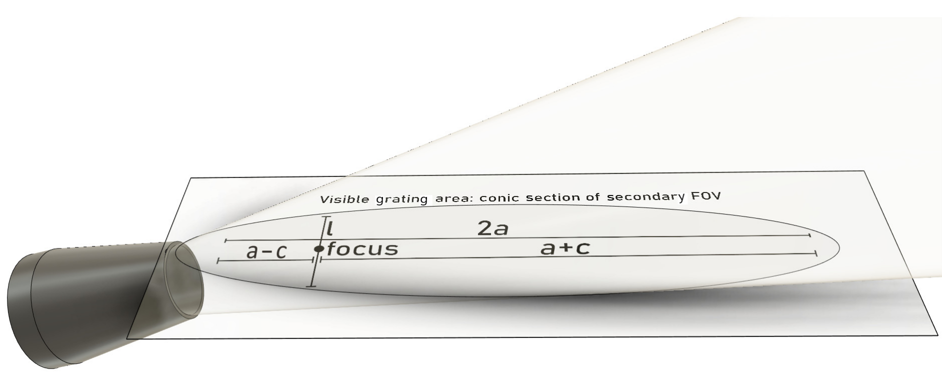

Fig. 4 Visible grating area as a conic section of secondary focusing element FOV. The secondary focusing element FOV is exaggerated in order to demonstrate that total collection area is truly a conic section. It is seen from this figure that the major axis is determined solely from the secondary aperture diameter and FOV, and the angle at which the secondary aperture axis intersects the grating.

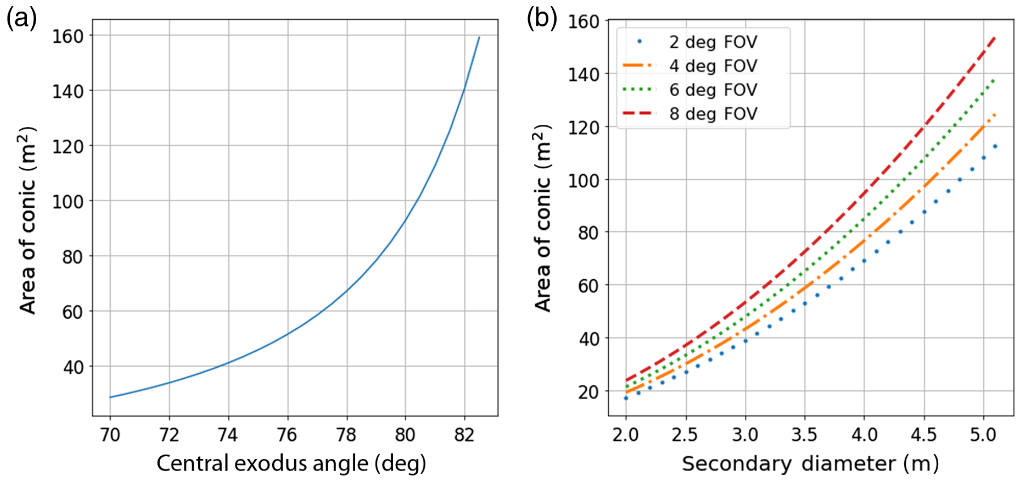

Fig. 5 (a) Total grating area visible to the secondary focusing element, taken as the conic section subtended by its FOV. The secondary focusing element is assumed to have a diameter of 2.5 m and FOV of 3 deg, characteristics analogous to the Sloan Digital Sky Survey telescope. As the exodus angle approaches grazing at 90 deg, the collection area is massively increased. (b) With the exodus angle constrained to 70 deg, the secondary focusing element characteristics are varied. Wider secondary diameters and FOVs also result in massively increased light collection area on the grating.

calculations. The ellipse of visible grating area is determined by the semimajor axis and semilatus rectum. These are given in terms of central exodus angle θ_E (the angle in which the secondary optical axis intersects the grating), secondary focusing element diameter D, and secondary FOV ϕ_{FOV}:

$$a = \frac{D}{2}\left(\sin(\pi/2 - \theta_E) + \frac{\cos(\pi/2 - \theta_E)}{\tan(\pi/2 - \theta_E - \phi_{\text{FOV}}/2)}\right). \tag{2}$$

$$l = \frac{D}{2}(1 + \frac{\tan(\phi_{\text{FOV}}/2)}{\tan(\pi/2 - \theta_E)}). \tag{3}$$

With these quantities in hand, we can determine the semiminor axis b and subsequently the total conic area A:

$$b = \sqrt{(l * a)}, A = \pi * a * b. \tag{4}$$

Figure 5 illustrates the scaling relationships of total conic area with the central exodus angle received by the secondary, as well as the diameter and FOV of the secondary focusing element. Figure 6 gives the required linear grating dimensions to inscribe (within a rectangular grating) the total visible conic area for a variety of secondary focusing element characteristics. In these figures, the central exodus angle is constrained to 70 deg.

3.2 *Wavelength-Dependent Light Collection Area and Bandwidth*

Though we have determined the total grating area visible to the secondary focusing element, the problem is far from being solved. Although the secondary focusing element can receive photons from all points in the FOV, only light of certain wavelengths will diffract from the grating at the necessary angle to enter the aperture of the secondary. Furthermore, the angle required to enter the secondary aperture depends on location within the visible grating area. It is for this reason that collection area must be treated wavelength by wavelength to get an accurate picture of the light collection area.

Light from an individual object within the observatory FOV is initially incident on the grating as a broadband coherent plane wave. After diffraction from the grating, the light is dispersed into many coherent plane waves exiting the grating in a wide range of angles at the corresponding

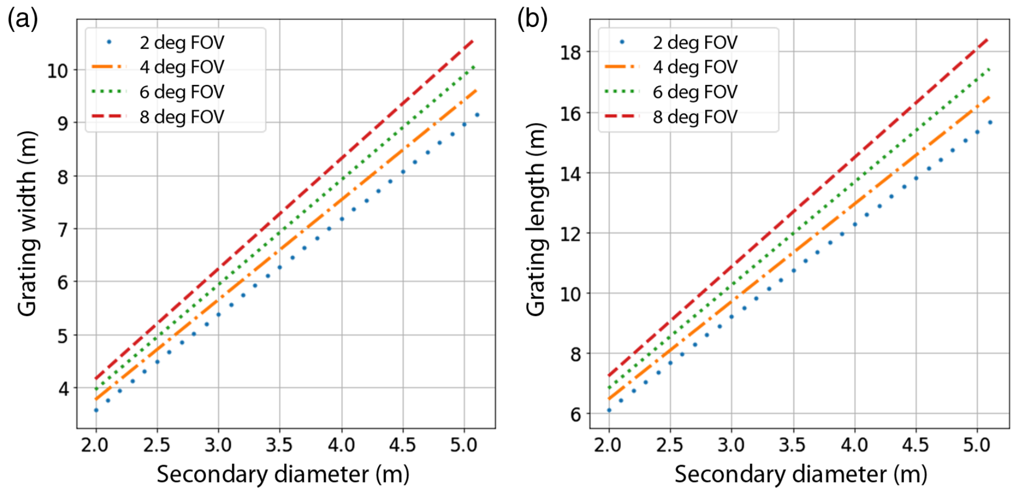

Fig. 6 Linear grating dimensions [width (2*b) and length (2*a), where a and b are the semimajor axis and semiminor axis, respectively] required to contain inscribed ellipse of visible grating area; shown as a function of the secondary focusing element diameter and FOV. In both panels of this figure, the central exodus angle is constrained to 70 deg.

wavelength [Eq. (1)]. The secondary focusing element positioned at grazing exodus is only able to capture a narrow-band slice of these diffracted wavefronts, as only wavefronts diffracted within the angular range of the secondary focusing element FOV can enter the secondary aperture. The wavelengths included in this narrow (single-object) band vary with angle in the sky along the direction of dispersion. The end result is that, for each diffracted wavelength (from a single object within the observatory FOV), there will be a grating subarea from which light enters the aperture of the secondary focusing optic. This subarea of the total conic sectional area corresponds to a particular wavelength and is determined from the cylindrical section subtended by the secondary focusing element aperture at the angle this light enters the secondary; this situation is illustrated in Fig. 7. Examples of light collecting area as a function of wavelength within the single-object bandwidth are given in Fig. 8.

Understanding the light collecting area for each object in the POG observatory FOV requires the application of a weighted average over these wavelength-dependent subareas, with weights corresponding to the spectral flux density of the observed object. In the interest of defining light collection power in all generality, we will assume a flat spectral flux density when computing the average collection area on the grating. This corresponds to conducting an unweighted average over all subareas over all wavelengths in the band. Analytically, this is represented by an integral over the FOV. For a given ellipse of semimajor axis a_λ and semiminor axis b_λ, we defined as a cylindrical section subtended by aperture diameter D at an exodus angle of θ_E. The average area over the single-object bandwidth $\langle A_\lambda \rangle$ may be found by integrating the cylindrical section over the valid range of angles $\theta_E - \phi_{\mathrm{FOV}}/2$ to $\theta_E + \phi_{\mathrm{FOV}}/2$:

$$\langle A_\lambda \rangle = \pi b_\lambda \langle a_\lambda \rangle = \pi \left(\frac{D}{2}\right) \frac{D}{2\phi_{\mathrm{FOV}}} \int_{\theta_E - \frac{\phi_{\mathrm{FOV}}}{2}}^{\theta_E + \frac{\phi_{\mathrm{FOV}}}{2}} \frac{\mathrm{d}\theta}{\cos(\theta)} = \frac{\pi D^2}{4\phi_{\mathrm{FOV}}} \ln\left(\frac{\tan\left(\frac{\pi/2+\theta_E+\phi_{\mathrm{FOV}}/2}{2}\right)}{\tan\left(\frac{\pi/2+\theta_E-\phi_{\mathrm{FOV}}/2}{2}\right)}\right). \quad (5)$$

Each output angle in the valid angular range from $\theta_E - \phi_{\mathrm{FOV}}/2$ to $\theta_E + \phi_{\mathrm{FOV}}/2$ corresponds to a single wavelength in the single-object bandwidth. A weight parameter may be incorporated into the integral by relating the diffraction angle and corresponding wavelength to the spectral flux density of the object in question. The unweighted calculation was conducted for a variety of secondary focusing element characteristics. Results of these calculations are given in the second panel of Fig. 9.

It is worth noting that Eq. (5) is formulated in the paraxial approximation of a diffraction grating. While a full analysis embodying nonparaxial diffraction theory[15] can be conducted, this

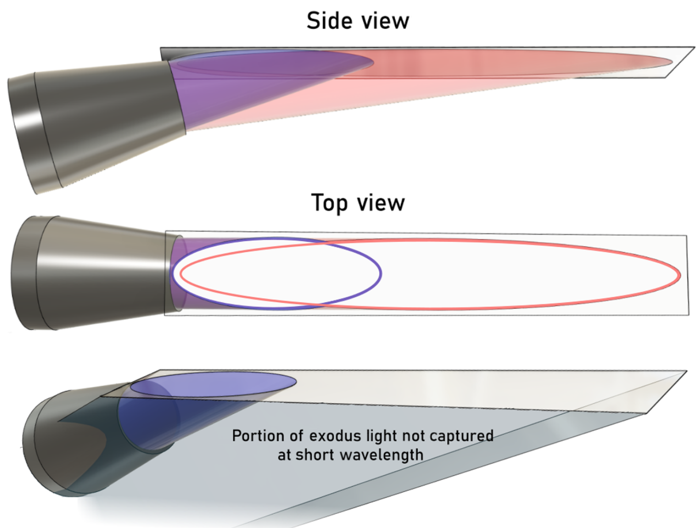

Fig. 7 The situation of Fig. 4 is reimagined in the case of multiple wavelengths, with the POG receiving light from a single-distant point source. After diffraction from the POG, every wavelength emanates from the grating at a different angle, and visible grating area varies across the spectral bandwidth for any given object in the observatory FOV. As such, collection area must be averaged over the wavelength dependent "subareas" of the visible conic area. For any given wavelength, the collection area is the cylindrical section subtended by the secondary focusing element diameter. Shorter wavelengths (blue) are received at smaller exodus angles and therefore have smaller cylindrical-section collecting areas than longer wavelengths (red). At shorter wavelengths, a significant portion of the exodus light may not be captured by the aperture of the secondary focusing element (displayed in the bottom row). However, for situations with a smaller (and more realistic) secondary FOV, the portion of lost light at short wavelengths will be much less than the exaggerated situation of this figure.

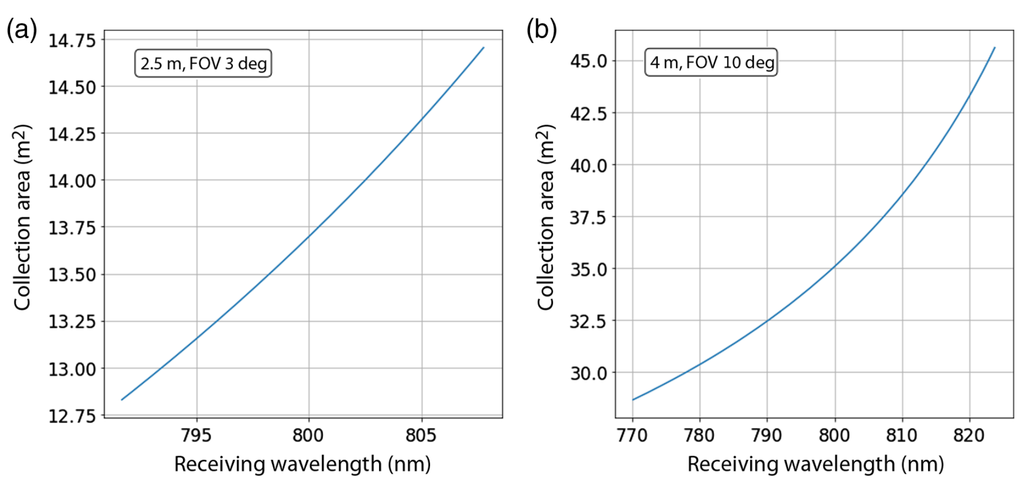

Fig. 8 Collection area as a function of wavelength for the case of two different secondary focusing elements. (a) A secondary focusing element of diameter 2.5 m and FOV 3 deg, whereas (b) has diameter 4 m and FOV 10 deg. Note that the FOV is specified because the limits of the FOV set the limits of the single-object bandwidth. The diameters and fields of view are very large in both cases; this is intended to maximize the number of photons collected (this will be elaborated on later). For both telescopes, the angle of incidence is 0 deg, and the receiving/exodus angle is 70 deg. We chose the grating spacing to ensure that the central wavelength would be 800 nm; in this case, the pitch is ~851 nm. Note that this figure gives the area of intersection of a cylinder with the grating (A_λ); the conic from a wide FOV would intersect a larger grating area, and collect light across the whole range of wavelengths. For an object at $\theta_{\text{in}} = 0$, wavelengths outside of the plotted range would not intersect the secondary focusing element at an angle that is within its FOV.

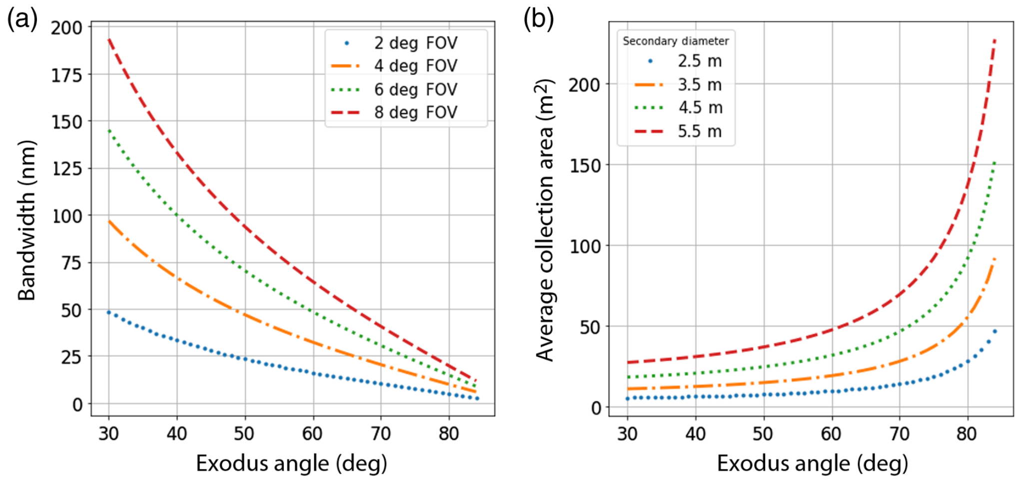

Fig. 9 (a) Single-object bandwidth as a function of exodus angle for a variety of secondary focusing optic fields of view. The telescope diameter is constrained to 2.5 m. Note the negative scaling of single-object bandwidth with increasing exodus angle. (b) Average collection area over the bandwidth, under the assumption of a flat spectral flux density, calculated as a function of central exodus angle for a variety of secondary focusing element apertures. The FOV is constrained to 3 deg. The positive scaling of collection area with exodus angle to the secondary focusing element is quite apparent. Taking both plots into consideration, it is clear that the large light collection areas of (b) are mitigated by the narrow single-object bandwidths of (a).

is left for later publications. Equation (5) therefore fails to fully realize the effects of incident light in the direction perpendicular to dispersion (the oblique direction). However, in a nonparaxial analysis, deviation of wavelength-averaged collection area from that given in Eq. (5) will be minor, since the cylindrical section subareas scale much more rapidly with angular changes in the diffraction direction as opposed to the oblique direction (due to the extreme tilt angle of the grating in the diffraction plane). This deviation will also be increasingly minor for smaller FOVs of the secondary focusing element, as the conic-sectional grating area becomes increasingly equal to the cylindrical section area as the secondary FOV decreases.

Given the impressive scaling of both the total conic sectional [Fig. 5(a)] and averaged cylindrical collection areas [Fig. 9(b)] with angle of exodus, one might assume that an arrangement with exodus angle close to 90 deg will yield the greatest number of collected photons. Sadly this is not the case, as the extremely high dispersion near grazing exodus results in narrowing of the bandwidth available to the observatory for any single source in the FOV. The functional relationship, derived directly from the grating equation, reads:

$$\Delta\lambda = p(\sin(\theta_E + \phi_{\mathrm{FOV}}/2) - \sin(\theta_E - \phi_{\mathrm{FOV}}/2)). \tag{6}$$

Application of this relationship to a sample of secondary focusing element characteristics and exodus angles yields Fig. 9(a). Note that this result is independent of grating efficiency, which could also vary as a function of exodus angle. Typically one might expect efficiency to decrease with increasing exodus angle, but this relationship would depend on the details of the grating itself (e.g., blaze angle and groove profile).

3.3 *Wavelength-Dependent Spectral Resolvance*

In Sec. 3.2, the collection area was seen to vary as a function of exodus angle/wavelength received by the secondary focusing element. Since the spectral resolvance of a grating in the first diffraction order is simply $R = N = L/p$ (the total number of illuminated fringes), the resolvance must also change as a function of exodus angle/wavelength. For a given exodus angle, the length of the illuminated portion of the grating is $L = D\ \sec(\theta)$. For a single object in the observatory FOV, the spectral resolvance will take the form:

$$R = N = \frac{D}{p}\sec(\theta), \tag{7}$$

where θ is a specific exodus angle from the grating (within the range $\theta_E - \phi_{\mathrm{FOV}}/2$ to $\theta_E + \phi_{\mathrm{FOV}}/2$), D is the diameter of the secondary focusing element, and p is the grating pitch. Equation (7) was obtained by substituting $L = D\,\sec(\theta)$, the major-axis of the cylindrical section subtended by the secondary aperture, into the resolvance equation.

In a more realistic scenario than the exaggerated example shown in Fig. 7, the secondary FOV will be small compared to the central exodus angle θ_E. Because the wavelength range of each object observed is small, the resolvance ($R = \lambda/\Delta\lambda$) does not vary much across the bandwidth. Because the exodus angle is the same regardless of angle of incidence, the resolvance of each object is similar, even though objects observed at various angles of incidence would be observed at different wavelengths.

3.4 *Field of View*

Although the addition of a POG to collect light does not significantly increase the number of photons collected, the high dispersion of the POG at grazing exodus does result in a massive increase to the FOV of the observatory. For any Dittoscope design composed of a secondary focusing optic/camera pointed at a plane grating, the observatory FOV along the axis of the grating is determined by the wavelength range in which observable sources emit, diffraction efficiency in the vicinity of the blaze angle (in the case of a blazed grating), and the free spectral range of the first diffraction order. Note that limitations of the free spectral range can potentially be overcome by the use of optical filtering and related techniques. The FOV perpendicular to the grating (oblique angles of incidence on the grating) is determined by the FOV of the secondary focusing element.

Though the specific application in question will ultimately determine the observatory FOV, an arbitrary wavelength range must be chosen in order to quantify the potential benefits of a POG design over conventional telescopes. If we assume a secondary focusing element with an FOV of 3 deg, and a desired wavelength range of 500 to 1100 nm, the overall observatory FOV is displayed in Fig. 10 as a function of exodus angle. The 500- to 1100-nm range is chosen to have some overlap with the spectral range of conventional optical telescopes but is consciously chosen

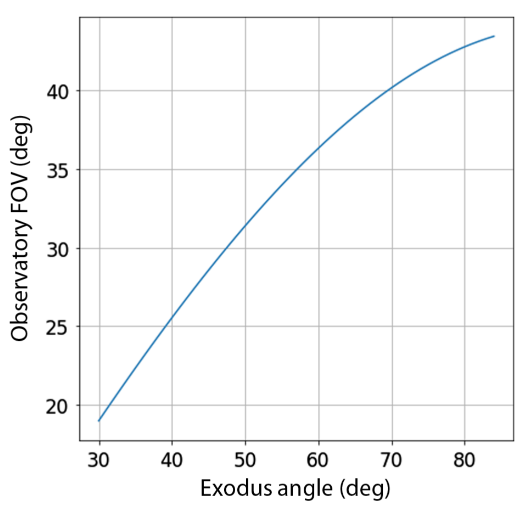

Fig. 10 Observatory FOV in the grating direction as a function of exodus angle, for the assumption of 3 deg secondary FOV and 500 to 1100 nm bandwidth. It is seen that the FOV in the direction of the grating is massively increased compared to that of the secondary focusing optic in isolation. Many potential Dittoscope applications hinge on this massively increased FOV as a method to survey a very large patch of sky. Note that the observed single-object bandwidth will vary along the angle on the sky aligned with the long axis of the grating.

to favor longer wavelengths, since large area gratings become increasingly difficult to manufacture with smaller groove-spacing (pitch).

The relationship between on-sky position and wavelength can be emphasized by further constraining the situation described in Fig. 10. Fixing the exodus angle at 70 deg necessitates a grating pitch of 851 nm, since the central wavelength (received at an incidence angle of 0 deg) is 800 nm. Figure 10 shows that a 70-deg exodus angle gives rise to a 40-deg FOV, resulting from a rearranged grating equation $\theta_{\text{in}} = \sin^{-1}(\lambda/851\ \text{nm} - \sin(70))$. When applied at the limits of our observable bandwidth of 500 to 1100 nm, a 500-nm central wavelength corresponds to sky objects with –20-deg incidence angle, and a 1100-nm central wavelength is received for objects at a 20-deg incidence angle. The per-object bandwidth for all objects within the FOV is found (by application of Eq. (6) to be $\sim$15 nm. The light received for objects in the angular range between -20 deg and 20 deg spans the observation bandwidth of 500 and 1100 nm.

Figure 10 demonstrates that high exodus angles result in a massively increased FOV relative to the secondary focusing element in isolation. This increase in FOV is among the most promising properties of the Dittoscope concept. Note, however, that the observed wavelength range for any individual source is quite narrow, and the detected wavelength varies over the entire detectable wavelength range, as a function of angular position in the sky along the long axis (dispersion direction) of the grating.

As mentioned in Sec. 3.2, the FOV is currently considered in the paraxial approximation of a diffraction grating. A grating in the paraxial approximation does not distort incident angles in the oblique (nondispersing) direction. Therefore, the observatory FOV in the oblique direction is currently taken to equal the FOV of the secondary focusing element. This approximation is accurate provided that the secondary focusing element possesses a narrow FOV in the oblique direction. Although a formulation encompassing nonparaxial (or conical) diffraction theory[15] is possible, it is not included in this discussion of the most basic aspects of a POG telescope.

3.5 *POG Figure of Merit: Spectral Étendue*

Among the most peculiar characteristics when assessing the merit of a hypothetical POG design is the rapid scaling of average collection area with exodus angle, coupled with the negative scaling of the per-object bandwidth (Fig. 9). Reduced bandwidth clearly leads to reduced photon flux, as a smaller slice of the spectral flux density is sampled for each object. This effect acts to offset the massive gains in light collecting area when moving to extreme exodus configurations.

This pair of counteracting scaling relationships inspires a new figure of merit similar to the widely used Otendue $= \Omega * A$, which quantifies the effectiveness of a conventional telescope in collecting photons. This is less useful for a POG observatory with a secondary focusing element at grazing exodus, since the étendue does not account for the severe restriction in the observable single-object bandwidth. Instead, we define a spectral étendue:

$$\text{spectral Otendue} = \Delta\lambda * \Omega * \langle A_\lambda \rangle. \tag{8}$$

With this definition, we calculate the spectral étendue for a sample of POG characteristics. The results are given in Fig. 11.

Figure 11(a) shows that spectral étendue exhibits only modest scaling with increasing exodus angle, demonstrating that the massive gains to collection area shown in Fig. 9(b) are largely subdued by the negative bandwidth scaling of Fig. 9(a). Rather than exodus angle, secondary focusing element characteristics of diameter and FOV emerge as the dominant factor in the scaling of spectral étendue [Fig. 11(b)]. However, the grating collects a large amount of light in an extremely narrow band. This property may preserve the POG as a potentially useful component for specific science objectives (e.g., faint high-resolution spectral features at high angular resolution).

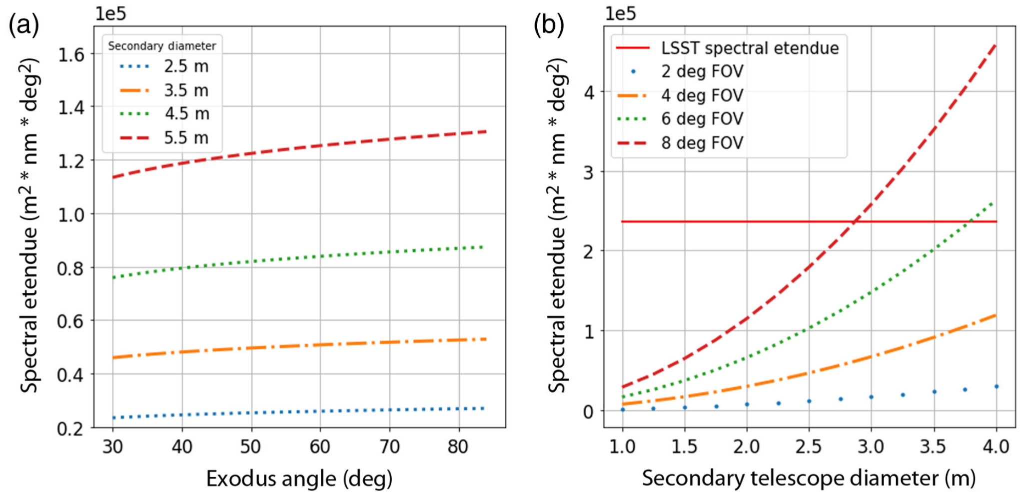

Fig. 11 (a) Spectral étendue as a function of exodus angle for a variety of secondary focusing optic diameters, a secondary focusing element FOV of 3 deg is assumed. Note the meager scaling of spectral étendue with exodus angle, resulting from the decreased single-object bandwidth in conjuction with increasing FOV and light collection area. (b) Spectral étendue as a function of secondary focusing optic diameter for a variety of secondary focusing optic FOVs, an exodus angle of 70 deg is assumed. The spectral étendue of LSST with no filter is given for comparison. Note the much more favorable scaling of spectral étendue with respect to the parameters of (b) in comparison to (a). It is apparent that secondary focusing element characteristics may play a more important role in Dittoscope performance than the exodus angle for a given configuration.

4 Angular Resolution of POG Telescopes

We show here that the angular diffraction limit is determined from the POG length and not by the size of the secondary focusing element. This is because the angular distance between two objects is magnified by the grating.[13]

4.1 *Diffraction Limit*

Imagine two objects that are separated by a small amount $d\theta_{\text{in}}$ and observed at the same wavelength. By taking the derivative of the grating equation [Eq. (1)] at constant wavelength, we find that

$$\frac{d\theta_{\text{out}}}{d\theta_{\text{in}}} = \frac{\cos(\theta_{\text{in}})}{\cos(\theta_{\text{out}})}. \tag{9}$$

In order to see this light on axis in the secondary focusing optic, $\cos(\theta_{\text{out}}) \sim D/L$, where L is the length of the grating intercepted by the secondary focusing element and D is the diameter of the telescope. For $\theta_{\text{in}} = 0$ deg, $Dd\theta_{\text{out}} = Ld\theta_{\text{in}}$. The diffraction limit (in terms of $d\theta_{\text{out}}$) of the secondary focusing element is proportional to the diameter of the telescope. However, if we map the angle that is seen by the secondary focusing element to the sky ($d\theta_{\text{in}}$), that diffraction limit is proportional to the length of the grating. So in the limit of perfect gratings and no atmosphere, the Dittoscope can resolve objects that are aligned along the length of the grating at the resolution of $d\theta_{\text{in}} \sim \lambda/L$.

This enhanced resolution is only realized in the dispersion direction of the grating. As a result, the point spread function (PSF) will be asymmetric in terms of on-sky angular coordinates. The physical PSF in the focal plane, however, will have the functional form of the secondary focusing element aperture. The position of the physical PSF in the focal plane will be asymmetric in terms of on-sky angular coordinates as they relate to the dispersion direction of the grating.

The angular magnification of the POG is similar to the angular difference magnification of conventional telescopes, which comes about as a consequence of conservation of étendue. The Dittoscope is not diffraction limited by the secondary focusing element aperture, in the same manner that an ocular equipped telescope is not diffraction limited by the pupil of the human eye.

4.2 *Atmospheric Seeing Simulations*

For a ground-based Dittoscope, one must consider the effect of the atmosphere on the wavefront that reaches the POG. At sufficient distance, the radiation from a star will form a plane wave that is incident on the Earth. However, the atmosphere will cause wavefront distortions in the light that actually makes it to the Dittoscope. Because the POG could potentially be tens or hundreds of meters long, it is much larger than the coherence length in the atmosphere. Therefore, the wavefront distortions will average out over the area of the POG, producing a blurring of the light from a point source that is similar to the "Airy disk" of a diffraction limited telescope (the time-averaged speckle distribution has the functional form of a diffraction limited PSF) but created instead from shifting diffraction patterns, or "speckles" that evolve on timescales of milliseconds.

To understand the effects of atmospheric seeing on the angular resolution of a ground based POG design, a simple simulation of atmospheric wavefront distortion was built to verify the seeing PSF predicted by theoretical considerations. This simulation generates sample wavefront distortions using emergent phenomena to mimic the pseudorandom distributions of turbulent cells in the upper atmosphere. Sample data were generated on a 10 m × 10 m grid with a grid spacing of 0.05 m. At initialization, random points of high wavefront distortion are injected into the grid and allowed to spread by repeated application of Gauss-Seidel relaxation. At each relaxation step, a random fluctuation of tunable magnitude occurs at each grid point. By tuning the number of relaxation steps, degree of fluctuation at each point, and the number/intensity of weighted points in the initialization grid, phase distributions heuristically similar (coherence length at each point in the grid) to real phase-screen data were generated. The sky was modeled from a contour plot of phase-screen data taken over a 12 m × 12 m area on Mauna Kea, Hawaii.[16]

With the grid of simulated phase-screen data generated, sample light rays were produced by applying a triangular mesh to the grid. The normal vector to each mesh face is used to determine θ_{in} in the grating equation. The resulting PSF in the focal plane can be visualized by a histogram of the angular distortions as calculated from the grating equation.

Figure 12 shows incident angle distortions generated from simulation data. The histograms of incident-angle distortion are equivalent to the distortion incurred by a 1 m × 100 m collector (or any other 100 m^2 primary grating), regardless of the fact that they are calculated from a 10 m × 10 m area; this is due to the isotropic nature of the wavefront distortions.

The seeing of, say, 1.5 arc sec becomes a blurring in the wavelength direction. In the case of our benchmark design, the wavelength blurring is ∼0.006 nm. The spot size that this produces after light from the secondary focusing element focal plane is dispersed with a second grating depends on how effectively the second grating reconstructs the sky. In principle, if a second spectrograph is capable of identifying the wavelength and position of every photon that hits the secondary focusing element focal plane, that wavelength blurring will turn back into a blurring in angle that is equal to 1.5 arc sec in the final image. That is because if you detected the wavelength exactly, you would know to within 1.5 arc sec where the photon originated. This blurring precludes diffraction limited imaging, as it does in all ground-based observations.

5 Disambiguating Objects in the Focal Plane

We now turn our attention to the endpoint of the optical system, the arrangement of detectors in the focal plane of the secondary focusing element. Observation of a large area diffraction grating by a conventional telescope results in a situation synonymous with the familiar "grism-image," in that each object is spread out into a spectrum in the grating direction. The difference between the sort of image received with a grating observed at a grazing angle, as opposed to a low-dispersion grism, is that there will be no chosen "central wavelength" with which to disambiguate positions of objects within the FOV. Furthermore, in configurations approaching grazing exodus, a vanishingly small portion of the object spectrum is spread across the entire detector in the dispersion

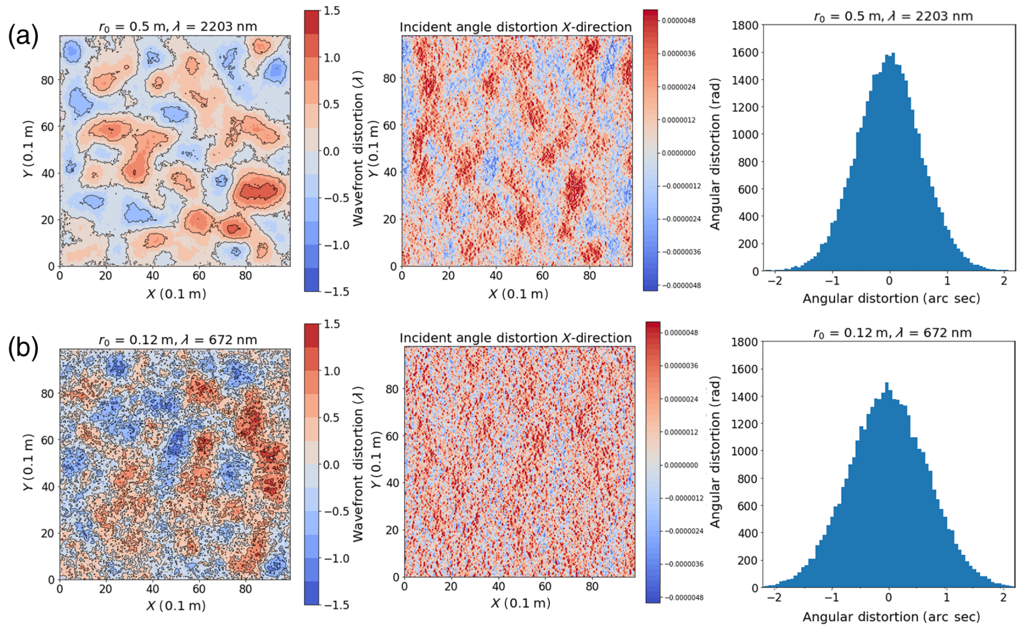

Fig. 12 Angular distortion for two simulations of differing coherence length under the same seeing conditions (coherence length is wavelength dependent). Theory dictates a coherence length of 0.5 m and wavelength of 2203 nm (a) should result in an angular resolution of 0.88 arc sec, and a coherence length of 0.12 m and wavelength of 672 nm (b) should produce an angular resolution of 1.12 arc sec. The rightmost plots demonstrate that the resulting angular distortion is in line with theoretical expectations.

direction. Objects that are aligned with the grating will overlap over the entire length of the FOV, which could be tens of degrees or more (see Sec. 3.4).

The discussion of Sec. 3.4 reveals that the single-object bandwidth is determined by the secondary FOV, in combination with the relevant wavelength range of observation/emission. The definition of single-object bandwidth as the wavelengths received at the margins of secondary FOV demands that the received light be spread across the entire detector plane defined by the secondary FOV. In this way, it could be extremely difficult to distinguish the true positions on the sky, as objects seen in the focal plane will consist of many overlapping spectra. In theory, this issue can be resolved if the wavelength of received light is known at every position in the detector plane, as each wavelength received at a unique angle by the secondary can be mapped to a unique location on the sky. This approach presents its own difficulties; to achieve the optimal angular resolution, the spectrograph used to disambiguate focal plane wavelengths must be of similar resolving power to the POG.

Highly chromatic effects also plague the imaging capability of large area zone-plate concepts.[4,5] In this case, a holographic "corrector" is often proposed as a sort of antifunction to the aberration incurred by the primary.[2,3] Unfortunately such an approach is likely impossible for POG designs, owing to the fact that there is no optical component that can act as an effective antifunction to the chromatic distortion introduced by the POG.

5.1 *Dual-Dispersion*

In THE MOST, a slit is placed at the focal plane of the secondary focusing element, oriented parallel to the grooves in the grating. Light from this slit is conveyed onto a secondary dispersing element. This technique, coined as dual dispersion, ensures that every location on the detector plane corresponds to a unique wavelength and position on the sky. However, this is only strictly true in the case of a single diffraction order, any application utilizing dual dispersion may require elimination of competing orders by specialized filtering schemes. POG configurations featuring extremely grazing exodus angles (e.g., THE MOST) will typically only have the second diffraction order competing with the first. The secondary dispersing element is shown conceptually in Fig. 2 as a prism in combination with an imaging camera. In practice, the secondary dispersing element would likely take the form of a conventional multiple-input spectrograph placed in the focal plane.

To measure all photons captured by the secondary focusing element (a condition assumed in all previous calculations), each pixel in the focal plane of the secondary must act as a slit or optical fiber, feeding into some sort of spectrographic instrument. The wavelength and direction from which each photon originated are disambiguated by dual dispersion. Although this technique is an elegant method for disambiguation of all photons received at the detection plane, it results in a colossal increase in the number of necessary pixels in the detector. In a normal telescope application, the number of pixels is set by the resolution and FOV; in a dual dispersion architecture, the number of pixels is compounded with the wavelength resolution and observation bandwidth:

$$\#\text{of pixels} = \frac{\pi}{4}\left(\frac{\text{secondary}_{\text{FOV}}}{\text{secondary}_{\text{resolution}}}\right)^2 * \left(\frac{\text{bandwidth}}{\lambda_{\text{resolution}}}\right). \tag{10}$$

The first two terms of Eq. (10) describe the number of pixels required for a conventional telescope (the secondary focusing element) to take full advantage of its diffraction limited angular resolution and FOV. The last term in Eq. (10) reflects the number of resolution elements required for the spectrograph to disambiguate the multiple wavelengths received from a wide swath of the sky in the direction of dispersion.

Drawing upon Figs. 6, 8, and 10, we can imagine a telescope consisting of a 2.5-m secondary focusing element with a 3-deg FOV, viewing an 8-m long grating at an exodus angle of 70 deg. If we set the observable wavelength range to 500 to 1100 nm (overall telescope bandwidth of 600 nm), the grating pitch is constrained to 851 nm by the grating equation. For this case, the FOV in the dispersion direction is 40 deg (again determined from the grating equation), leading to an overall FOV of $40\ \text{deg} \times 3\ \text{deg}$. The resolvance of a grating in the first diffraction order is equal to the number of diffraction fringes. For the case of an 8-m grating with 851 nm pitch, we arrive at a resolvance of $\sim 9.4 \times 10^6$, and a minimum resolvable wavelength difference of $\sim 5.3 \times 10^{-5}$ nm. The diffraction limited angular resolution of the secondary focusing element, which corresponds to the observatory resolution in the nondispersing direction, is $\sim 1.4 \times 10^{-5}$ deg [this is the angular resolution at the high frequency side (500 nm) of the observation bandwidth]. Taking these quantities into account, we arrive at

$$\#\text{of pixels} = \frac{\pi}{4}\left(\frac{3\ \text{deg}}{1.4 \times 10^{-5}\ \text{deg}}\right)^2 * \left(\frac{600\ \text{nm}}{5.3 \times 10^{-5}\ \text{nm}}\right) \approx 10^{17}. \tag{11}$$

This is undoubtedly an unreasonable quantity of pixels, especially considering that in a dual-dispersion architecture, the overwhelming majority of these pixels will capture no photons. This calculation is performed under the assumption that all photons incident on the focal plane of the secondary are successfully disambiguated by dual dispersion. In this view, each pixel in the focal plane of the secondary represents a single "slit" or spectrographic fiber, which is subsequently fed into some sort of extremely high-resolution spectrograph.

This calculation assumes that the full angular resolution of the POG and the secondary focusing element is achieved. Although this situation is likely impossible, it serves as an upper bound to the number of pixels required. It is worth noting that a particular Dittoscope application may not require the full resolution limits of the observatory. Limiting the resolution could considerably reduce the number of pixels, provided the science objectives in question do not require the full spectral/angular resolution available. Note, however, that the resolution in wavelength and angular sky position in the dispersion direction are tied together, so one cannot simply choose to lower their resolution independently. Also some imperfections in the grating will impact the resolution in angular position, most notably errors in groove quality and pitch regularity.

In the previous example, the upper limit on the number of required pixels was informed by the physical size of the POG and secondary under the assumption of ideal angular resolution. If, instead, the science objectives inform the required resolution, we can construct an application in which dual dispersion requires fewer pixels to disambiguate incident photons. One example is the use of the POG for its large FOV rather than high resolution (Sec. 6.2). If a given science objective only required an angular resolution of 0.1 deg, then (assuming the same arrangement as the previous example), the ∼40 deg × 3 deg swathe of sky would require ∼12,000 pixels to represent each area of the sky (it is worth noting that this situation requires asymmetrical slits/fibers in the focal plane of the secondary focusing element). Plugging a 0.1-deg difference into the grating equation yields a required spectrograph resolution of ∼1.5 nm, and the number of pixels in each spectrograph channel would be ∼400 based on the 600-nm bandwidth of this arrangement. The number of required pixels for this hypothetical arrangement is ∼5 million, which is easily achieved with current detector technology.

6 Discussion: Reaping the Benefits of POG Designs

We have shown that POG observatories present uniquely challenging properties. Massive increases in FOV and collection area (relative to the secondary focusing element in isolation) are coupled with a decreased per-object bandwidth and difficulty in disambiguating photons in the focal plane. The results of Sec. 3.5, namely the plot of spectral étendue in Fig. 11, demonstrate that only meager scaling of this figure of merit is achieved by approaching a grazing exodus configuration. Our results suggest that if the only goal is to collect as many photons as possible (that are undifferentiated by wavelength), it is simpler and more cost effective to use a conventional telescope rather than a POG observatory.

Given this distinction, is it possible to design a POG observatory that is competitive with conventional technology? Novel POG architectures may be useful for a variety of highly specialized science objectives. Any given Dittoscope design is not likely to be a generalist instrument, but for applications requiring extremely large FOVs, high angular resolution, multiple-object high-resolution spectroscopy, or low aerial mass, a POG design may prove extremely competitive.

6.1 *High Angular Resolution*

In Sec. 4, it was shown that POG telescopes possess angular resolution equal to that of a conventional telescope with diameter equal to the grating length. For a space-based POG observatory, this presents a unique low-mass solution to observations requiring extremely high angular resolution (e.g., extrasolar planet observations, as described in a proceedings publication on the Diffractive Interfero Coronagraph Exoplanet Resolver[17]). This extremely precise angular resolution is only realized in one dimension, and only for a small bandwidth (typically on the order of nanometers). Any science objectives seeking to utilize this one-dimensional resolution will require POG architectures and observational strategies designed to work around these limitations.

6.2 *High Field of View*

If attention is shifted away from angular resolution in favor of the massive increase to the FOV outlined in Sec. 3.4, a ground-based observatory becomes an intriguing possibility. The natural application for a high FOV low single-object bandwidth observatory is situational awareness (i.e., detection of near Earth objects as described in a proceedings publication on Trip Wire Optics[18]). One challenge encountered with this application is disambiguation of focal plane objects with a reasonable number of detector pixels, a problem which has not been solved as of the time of this publication. Another challenge is the limit on angular resolution imposed by seeing without the aid of adaptive optics, as discussed in Sec. 4.2.

6.3 *High Spectral Resolution: Radial Velocity Measurements*

All POG observatories will typically feature extremely high spectral resolution, with this resolution being proportional to the grating length. This extremely high spectral resolution is generally taken in a vanishingly small bandwidth for any single source, requiring highly specific and narrow spectral features to be a useful property.

A natural application is that of radial velocity measurements of stellar spectral lines. This approach may allow a Dittoscope to discover new exoplanets by the radial velocity method and measure exoplanet masses for those that were discovered by their transits. If high enough spectral resolution can be achieved, a Dittoscope could possibly be used to map the accelerations of stars in the Milky Way. If the accelerations of stars within the Milky Way were known at the level of cm/s, new limits could be placed on the distribution of dark matter in the Galactic halo. In addition to technical feasibility of high resolution, we would also need to address issues of intrinsic line width and stability in astronomical objects, which is usually addressed by simultaneous observation of multiple lines.

6.4 *Rotating POG Observatories: Spectrographic Surveys*

The narrow bandwidth properties of many POG arrangements could in theory be solved by operating the telescope in a mode analogous to a "drift scan." By allowing the POG observatory to slowly rotate by means of orbital motion, the Earth's rotation, or by manual adjustment, the full spectrum of all objects could be built up over the course of a full transit. In a conventional telescope, all objects in a small FOV are captured with a large bandwidth, a drift scan serving to image more objects. A POG observatory takes a different approach, with many objects in a wide FOV captured in a sequence of narrow high-resolution bands, the drift scan serving to build up a wider spectrum for each object. Using such a technique, a spectral survey could be accomplished with little or no active pointing of the observatory.

6.5 *Future Considerations*

In these analyses, many important features and requirements of POG technology have not been fully addressed. Among the most important unaddressed considerations are as follows.

- Optical efficiency of diffraction gratings at or near grazing exodus:
  Many efficiency characteristics depend upon a variety of factors including the wavelength range in consideration, angle of exodus, blaze angle, optical thin-films/coatings, and whether the grating is holographic or surface relief.
- Manufacture of large area diffraction gratings:
  Current state-of-the-art methods[19] can produce gratings of area $\sim 1\ \mathrm{m}^2$ via reactive ion etching (RIE) techniques. However, these methods are currently incapable of producing larger gratings. New methods of manufacture (e.g., large area holography or RIE) must be developed for many Dittoscope concepts to become viable.
- Optical characteristics:
  Surface figure tolerance must be characterized. The effective Airy PSF after focusing from a large area grating remains to be fully understood. Laboratory experiments must be devised to address these concerns. Issues of efficiency at grazing, line spacing tolerance, and groove profile/blazing have yet to be fully explored for this arrangement.
- Detectors:
  Many Dittoscope architectures may require light detection at the single-photon level. Many emerging technologies, such as the skipper CCD[20] and transition edge sensor bolometer,[21] may enable POG technology in the coming years.

In order for POG technology to be fully realized as a feasible concept, all of the above requirements must be addressed in future works.

7 Conclusion

The basic telescope design consists of a long flat POG that diffracts light into a secondary focusing element of specified diameter and FOV. In the focal plane of the secondary optic, a small wavelength range of each observed object is spread out in the dispersion direction of the grating. The position of the spectrum depends on the angular sky position in the oblique direction perpendicular to the dispersion direction of the grating. The wavelength range depends on the angular sky position in the dispersion direction of the grating. Position in the sky in the dispersion direction can be determined if the wavelengths are separated by an additional disperser.

In addition to considerations for specific applications, we have approached the analysis of nonfocusing POG telescopes from a broad and general standpoint, seeking to find basic metrics for comparing POG technology to more conventional astronomical observatories. In our analyses, we have attempted to make as few assumptions as possible regarding the components of the optical system, and set constraints on the secondary focusing element only when strictly necessary. Using this approach, we have derived many simple relationships connecting a Dittoscope's most basic physical parameters to useful metrics quantifying its ability to collect astronomical photons as follows.

- In principle, dispersion of POGs observed at grazing exodus is extremely high; R is formally in the millions for grating lengths in excess of several meters. Extremely high-resolution spectra could be contemplated.
- The use of a nonfocusing POG at grazing exodus for optical leverage drastically increases the light collection area over that of the secondary focusing element alone. However, this large area collects photons in a small bandwidth for each object, and the observed wavelength range varies across the sky.
- Evaluation of the wavelength-dependent light collection area, observatory FOV, and single-object bandwidth led to the definition of a spectral étendue $(\Delta\lambda * \Omega * \langle A_\lambda \rangle)$; a useful metric for evaluating the light collection efficiency of a Dittoscope.
- The spectral étendue scales with secondary focusing element characteristics of diameter and FOV, rather than the properties or position of the POG itself. This result is surprising considering the massive increase in collection area achieved at grazing exodus. However, the increase in collection area is effectively subverted by narrowing of the single-object bandwidth.
- Dittoscopes exhibit a massively increased FOV compared to the secondary focusing element in isolation. An FOV in excess of 40 deg is theoretically possible. Note, however, that this FOV is observed in different wavelength ranges in the dispersion direction of the grating.
- The angular resolution (in the direction of dispersion) of a POG at grazing exodus is proportional to the grating length. The proportionality relationship is conceptually similar to the angular enhancement properties of a conventional telescope from conservation of étendue. The diffraction limit in the dispersion direction is $\sim\lambda/L$. This could make a Dittoscope an attractive option for applications requiring extremely high resolution.
- Atmospheric seeing has similar effects on a ground-based POG telescope as it does on a conventional ground-based telescope. In order to capitalize on the full angular and spectral resolution available to the POG, a Dittoscope must be placed in space.
- Due to the multiple overlapping spectra in the focal plane of the secondary focusing element, disambiguation of focal plane objects is a major problem for theoretical POG applications. Dual dispersion is currently the only known method for disambiguating all photons received at the focal plane. However, choices must be made to avoid requiring an unreasonable number of pixels in the detector.

Given these findings, we suggest a few circumstances in which nonfocusing POG telescopes might be advantageous. The potential for low aerial mass deployment of POG observatories in space might enable cost competitive missions that are impossible to achieve using a conventional telescope. Applications necessitating extremely high spectral resolution, wide FOV, low aerial mass, or extremely high angular resolution are well suited to benefit from an application of POG technology.

Acknowledgments

This work was supported by NASA Innovative Advanced Concepts (NIAC) Phase II (Grant No. 80NSSC19K0973), Manit Limlamai, and a fellowship from the NASA/NY Space Grant.

References

1. A. V. Baez, "Fresnel zone plate for optical image formation using extreme ultraviolet and soft x radiation," *J. Opt. Soc. Am.* **51**, 405–412 (1961).

2. K. C. Johnson, "Dispersion-compensated Fresnel lens," US Patent 5,161,057 (1992).
3. D. Faklis and G. M. Morris, "Broadband imaging with holographic lenses," *Opt. Eng.* **28**(6), 592–598 (1989).
4. R. A. Hyde et al., "Eyeglass: a very large aperture diffractive space telescope," *Proc. SPIE* **4849**, 28–39 (2002).
5. H. A. MacEwen and J. B. Breckinridge, "Large diffractive/refractive apertures for space and airborne telescopes," *Proc. SPIE* **8739**, 39–54 (2013).
6. G. Andersen and D. Tullson, "Broadband antihole photon sieve telescope," *Appl. Opt.* **46**, 3706–3708 (2007).
7. L. Koechlin, D. Serre, and P. Duchon, "High resolution imaging with Fresnel interferometric arrays: suitability for exoplanet detection," *A&A* **443**(2), 709–720 (2005).
8. A. J. Wesselink, "Astronomical objective gratings," *Appl. Opt.* **3**, 889 (1964).
9. E. Hertzsprung, *Astron. Nachr.* **186**, 177 (1910).
10. J. M. Hill et al., "Multiple object spectroscopy: the medusa spectrograph," *Astrophys. J.* **242**, L69–L72 (1980).
11. T. Ditto, "The dittoscope," *Proc. SPIE* **4840**, 586–597 (2003).
12. T. D. Ditto and J. M. Ritter, "Million object spectrograph," *Proc. SPIE* **7018**, 70182R (2008).
13. T. D. Ditto, "Conservation of étendue in a primary objective grating telescope," *Proc. SPIE* **9151**, 91515T (2014).
14. T. D. Ditto, "The High Étendue Multiple Object Spectrographic Telescope," NASA Innovative Advanced Concepts (NIAC) Research Award No. 80NSSC19K0973, 2022, http://www.3dewitt.com/PDF/Ditto_Final_Report_NIAC_Phase_II-THE_MOST.pdf
15. J. E. Harvey and C. L. Vernold, "Description of diffraction grating behavior in direction cosine space," *Appl. Opt.* **37**, 8158–8159 (1998).
16. J. D. Monnierr, "Optical interferometry in astronomy," *Rep. Prog. Phys.* **66**, 789 (2003).
17. H. J. Newberg and L. A. Swordy, "Diffractive interfero coronagraph exoplanet resolver (DICER): detecting and characterizing all Earth-like exoplanets orbiting Sun-like stars within 10 pc," *Proc. SPIE* **12180**, 121805E (2022).
18. H. J. Newberg, L. Swordy, and T. D. Ditto, "Feasibility of NEO detection with a primary objective grating telescope," *Proc. SPIE* **11445**, 114452I (2020).
19. B. Xu et al., "Reactive ion beam etching of large diffraction gratings," in *Proc. 50th Annu. Tech. Conf. Soc. Vac. Coaters*, pp. 369–376 (2008).
20. J. Tiffenberg et al., "Single-electron and single-photon sensitivity with a silicon skipper CCD," *Phys. Rev. Lett.* **119**, 131802 (2017).
21. P. C. Nagler, J. E. Sadleir, and E. J. Wollack, "Transition-edge sensor detectors for the origins space telescope," *J. Astron. Telesc. Instrum. Syst.* **7**, 011005 (2021).

Leaf Swordy received his BS and MS degrees in physics from Rensselaer Polytechnic Institute in 2018 and 2019, respectively. He is a doctoral student at Rensselaer Polytechnic Institute. With a background in high-purity liquid noble gas systems and general R&D for the XENON1T and nEXO experiments, his research now centers on theoretical telescope architectures utilizing holographic primaries, namely the diffractive interfero coronagraph exoplanet resolver.

Heidi Jo Newberg is a professor in the Physics Department at Rensselaer Polytechnic Institute. She contributed to the Supernova Cosmology Project, the Sloan Digital Sky Survey, and the Chinese LAMOST Project, and she currently runs the MilkyWay@home volunteer supercomputer. She has published in diverse areas of astrophysics including discovery of tidal streams in the Milky Way halo and disequilibrium in its disk, supernova searches, discovery of dark energy, the spatial distribution of dark matter, and now Dittoscopes.

Thomas Ditto is an inventor and artist who proposed the "Dittoscope" in 2002. It derived from a microscope of similar design which used grazing incidence as leverage. By reversing the angles of input and output, the leverage shifted from microscopic examination to astronomical. Subsequently, the microscope was developed under research support from the NSF, and the telescope has been studied under a fellowship from NIAC.